ELSEVIER

Physics of the Earth and Planetary Interiors 128 (2001) 195–205

PHYSICS OF THE EARTH AND PLANETARY INTERIORS

www.elsevier.com/locate/pepi

The influence of boundary heterogeneity in experimental models of mantle convection with internal heat sources

A. Namiki*, K. Kurita

Department of Earth and Planetary Science, University of Tokyo, 7-3-1 Hongo, Bunkyo, Tokyo 113-0033, Japan

Received 31 December 2000; accepted 14 August 2001

Abstract

The lateral variations in the thickness of the D″ layer observed by recent global seismology are suspected to control mantle dynamics. Namiki and Kurita (1999) performed laboratory experiments to explore how undulations of various sizes in the D″ layer affect convection patterns. In addition, we found that the undulation at the lower boundary can induce plumes and that there is a critical height above which the undulation controls convection patterns. Observed undulations at the top of the D″ layer exceed this critical height, suggesting that they may control the mantle convection patterns. The previous work, however, assumed basal heating. Since internal heating is an important source which drives mantle convection, we extend our previous study to a case incorporating internal heat sources using laboratory experiments. Internal heat generation is simulated by lowering the boundary temperatures at a constant rate. We observed that the undulation, which has the comparable thickness to the critical height determined in the purely basal heating case, can fix the location of the upwelling although the magnitude of the intensity of the upwelling is weaker. This situation is similar to the Earth's hotspots and suggests that the undulation at the top of the D″ layer is the source region of the hotspots.

Keywords: Internal heating; D″ layer; Hotspots; Mantle convection

1. Introduction

Several recent seismological discoveries have revealed the presence of stratification of the D″ region in many areas, with 1.5–3% velocity discontinuities for both compressional (P) and shear (S) waves at depths of 150–400 km above the CMB, and revealed the presence of strong heterogeneity at a variety of scale lengths in D″ layer (e.g. Lay et al., 1997; Garnero, 2000). Because of its strong horizontal heterogeneity and its distribution in correlation with the location of the ancient fossil slab (Wysession, 1996), the D″ layer is regarded as a chemically separated layer. Although the discontinuous structure is sometimes related with a phase change (Sidorin et al., 1999), the mineral that could be a candidate of the phase change has not been identified (Serghiou et al., 1998).

The existence of a chemically separated D″ layer means that the lower boundary of the mantle convection corresponds to the top of the D″ layer. In this context, lateral variations in the thickness of the D″ layer, observed by recent global seismology (e.g. Kendall and Shearer, 1994; Wysession et al., 1998), are the topographical undulation imposed at the lower boundary of mantle convection. The undulation will affect the convection pattern of the mantle. Actually, some laboratory and numerical experiments have shown that the chemically separated dense layer makes undulations at the boundary (e.g. Hansen and Yuen, 1988; Olson and

* Corresponding author.
E-mail address: namiki@sys.eps.s.u-tokyo.ac.jp (A. Namiki).

0031-9201/01/$ – see front matter
PII: S0031-9201(01)00286-2

Kincaid, 1991). Besides, some numerical experiments show the coupling structure between the topographical undulations and the upwellings (Kellogg, 1997; Montague et al., 1998; Tackley, 1998; Montague and Kellogg, 2000).

Namiki and Kurita (1999) performed laboratory experiments to explore how the undulations of various sizes in the D″ layer affect the mantle convection patterns and found that the undulations can induce plumes if the amplitude of undulation is above the critical height. Observed undulations at the top of the D″ layer exceed this critical value, which suggests that they may control mantle convection patterns. The previous work, however, assumed basal heating. Since internal heating is an important source that drives mantle convection, we extend our previous study to a case incorporating an internal heat source.

The pattern of internal heating convection is more time-dependent than that of the basal heating case; i.e. the sites of downwellings are closely spaced, and the locations are time-dependent. The convection pattern shows little or no long-lived coherent structure (Houseman, 1988; Parmentier et al., 1994). Convection heated partly from within and partly from below has been investigated numerically (Houseman, 1988; Bercovici et al., 1989; Travis et al., 1990; Sotin and Labrosse, 1999) and experimentally (Weinstein and Olson, 1990). They showed that upwellings become fainter like return flow to downwellings, as internal heating rate increases. Since the mean temperature of the convection cells systematically increases as a function of the internal heating rate (Sotin and Labrosse, 1999), the lower thermal boundary layer at a high internal heating rate does not have enough temperature differences to generate buoyancy for a vigorous plume. Thus, it is not obvious whether the undulation at the lower boundary can make a vigorous ascending region under a partly internal heating case.

There are two possible effects of internal heating in controlling convection though undulations on the lower boundary. One is that the effect of the undulation becomes weaker. When the internal heating is vigorous, the lower thermal boundary becomes less distinctive. This makes the upwelling weaker because the fluid near the lower boundary cannot get enough localized thermal buoyancy. In this context, for the undulation on the lower boundary, a weaker effect is expected in internal heating than in the purely basal heating case. The other possibility is that the convection pattern becomes more sensitive to the undulation. In the basal heating case, we observed that the time-dependent convection was more sensitive to the undulation than the steady-state convection, which indicates that the unsteadiness makes the convection sensitive to undulations. Since internal heating makes the convection pattern unsteady, we can infer that the convection system becomes sensitive to undulations.

The goal of this paper is to clarify whether the topographical undulation on the lower boundary can affect the mantle convection pattern under a partially internal heating situation.

2. Experimental settings

2.1. The method of internal heat production

Internal heat generation is simulated by lowering the boundary temperatures at a constant rate. This method was introduced by Krishnamurti (1968a), Krishnamurti (1968b). The detailed derivation of governing equations for simulating the convection with internal heat production by the lowering of the boundary temperature has been provided in Weinstein and Olson (1990). The definitions of some parameters are included here.

In this technique, the Rayleigh number based on the imposed temperature difference between the upper and lower boundaries (Ra_T) is defined by

$$Ra_T = \frac{\alpha g \, \Delta T d^3}{\kappa \nu} \tag{1}$$

where α is the coefficient of thermal expansion, g the gravitational acceleration, ΔT the temperature difference across the fluid layer, d the thickness of the convection layer, κ the thermal diffusivity, and ν is the kinematic viscosity. The equivalent Rayleigh number for internal heat generation in the case of this simulation, Ra_H, is given as follows:

$$Ra_H = -\frac{\alpha g d^5}{\nu k \kappa} \rho C_p \frac{\partial T_s}{\partial t} \tag{2}$$

where k is the thermal conductivity, ρ the density, C_p the specific heat at constant pressure, and T_s is the temperature at the surface boundary. Here, $\partial T_s/\partial t$ means temperature lowering, and $-\rho C_p(\partial T_s/\partial t)$ cor-

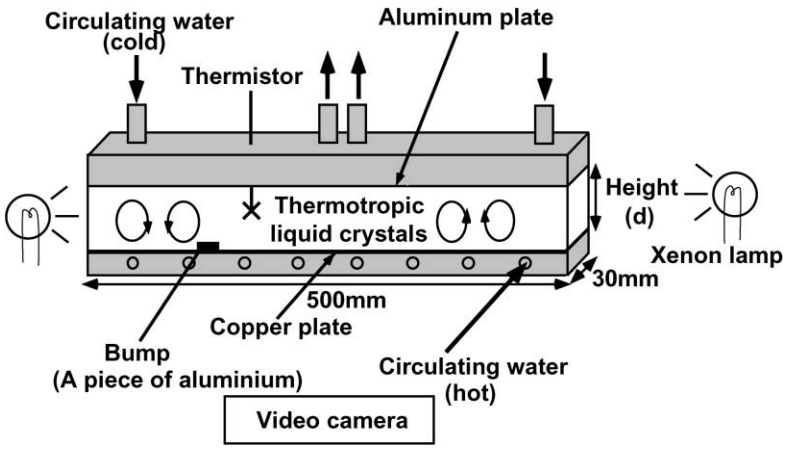

Fig. 1. Sketch of the experimental apparatus.

responds to the volumetric internal heat generation. The volumetric heat production rate normalized by the conductive heat flux is written as

$$R = -\frac{d^2}{\kappa \Delta T}\frac{\partial T_s}{\partial t} \tag{3}$$

2.2. Experimental apparatus and conditions

The experimental apparatus used in this work is fundamentally similar to that stated in Namiki and Kurita (1999) and is depicted in Fig. 1. The experimental tank is rectangular (500 mm long by 30 mm wide with a variable depth between 52 and 60 mm). The tank is heated from below and cooled from above. The temperatures of the upper and lower boundaries are controlled by circulating water. Glycerol solution is used as the working fluid. The Rayleigh number is varied by changing the concentration of glycerol, the depth of the convection height, and the temperature difference between the upper and lower boundaries. The temperature fields are visualized by thermotropic liquid crystal powder, which changes its reflective color within the prescribed temperature range. Light passed through a slit illuminates the fluid in cross section. Since the effective range of the temperature for thermotropic colorization is smaller than the imposed temperature range, we blended two kinds of micro-powder having different colorization temperatures. The temperature fields at the beginning and ending stages of the experiments can be observed. To investigate the effects of boundary undulation, we inserted a piece of aluminum block on the lower boundary as an isothermal rigid bump. We monitored the temperatures of the circulating water and the glycerol layer using five thermistors.

The process of inserting the bump and lowering the temperature is as follows. First, the temperature of the upper and lower boundaries was kept constant until the convection pattern reached equilibrium. This was confirmed by visual observations of convection patterns using one kind of thermotropic liquid crystals. Here, we inserted a bump at the location of the downwelling site. Next, we started to lower the boundary temperatures at a constant rate. The temperature of the fluid layer is once out of the range where the thermotropic liquid crystal reflects the color, which makes the convection pattern non-observable. When the temperature of the fluid layer reached the temperature range of another thermotropic liquid crystal, the convection patterns could be observed again.

The experimental conditions are reported in Table 1. The Rayleigh number and the Prandtl number vary within a single experiment, because the temperature range must be wide in order to lower the upper and lower boundary temperatures and the viscosity of glycerol depends on the temperature. The maximum and minimum Ra_T and Ra_H and the minimum and maximum Pr correspond to the beginning and the end of each experiment, respectively. The ratio of internal heating (%) is calculated by the $R/(R+Nu)$, where Nu is the Nusselt number. Nu is estimated by

Table 1
Experimental conditions[a]

	(a) and (b)	(c) and (d)
Ra_T	6×10^4–3×10^4	6×10^6–5×10^6
R	6	7
Ra_H	4×10^5–2×10^5	4×10^7–3×10^7
$\partial T_s/\partial t$ (K/s)	10^{-3}	2×10^{-3}
Ratio of internal heating (%)	70	40
Pr	3000–6000	100–200
Height of the bump	0.1	0.03
δ_{th}^2/κ (min)	8–12	0.7–0.8

[a] The boundary conditions of (a), (c) are homogeneous, and (b), (d) show a bump. Other states of (a), (b) and (c), (d) are the same, respectively (see text for more details).

$0.161Ra_T^{0.281}$ (Shen et al., 1996) and indicates the normalized heat flux due to basal heating. Since addition of internal heating will decrease Nu, this estimation shows the minimum content of internal heating. δ_{th}^2/κ is the characteristic time scale for the growth of the thermal boundary layer. To calculate the thickness of the boundary layer, we adopted the formulation of $\delta_{th} \sim d/(2 \times Nu)$, which is based on the basal heating convection. The height of the bump is normalized with the depth of the convection layer.

The estimated Reynolds number ($Re \sim va/\nu$) is smaller than 1. To calculate Re, the plume-head radius is selected as a characteristic length scale. The measured maximum plume-head size, maximum rise speed, and kinematic viscosity are $a = 10\,\mathrm{mm}$, $v = 1\,\mathrm{mm\,s^{-1}}$, and $\nu = 1.3 \times 10^5\,\mathrm{m^2\,s^{-1}}$, respectively, at $Ra_T \sim 5 \times 10^6$. In this case, viscous effects are dominant over inertial effects.

3. Results

Fig. 2 is the overlay of the experimental setting in this work to that of the previous work (Namiki and Kurita, 1999). In the basal heating case, the critical height at which the bump affects the convection pattern is a function of Ra_T and the convection pattern. When the convection is at the steady state, the critical height is determined by the thickness of the thermal boundary layer. When the convection pattern is time-dependent for higher Ra_T, the critical height is smaller than the thickness of the thermal boundary layer. We selected the height of the bump to be the same order of the critical height determined by the basal heating case at the regime of time-dependent convection.

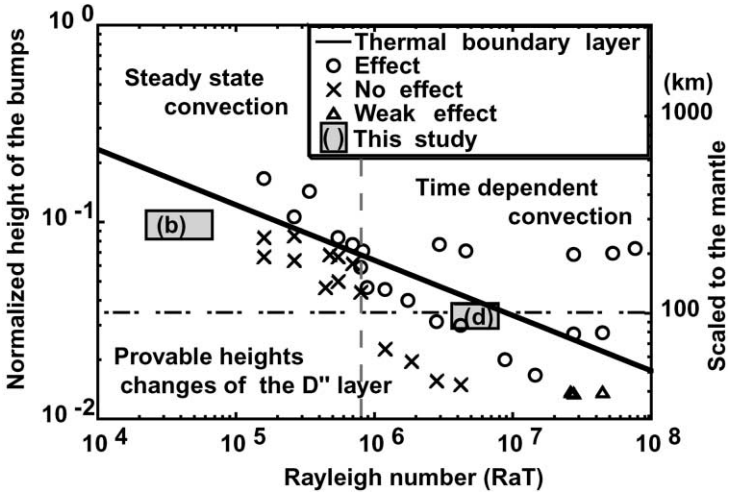

Fig. 2. Phase diagram of the effect of the bump. x-, left y-axis, and right y-axis show the Rayleigh number, the bump height normalized by the height of the convecting layer, and the corresponding height for Earth's mantle, respectively. Rectangles indicate state of this work. Others are based on our previous work (Namiki and Kurita, 1999) for the basal heating case. The symbol (○) denotes the case when the bump affects the convection pattern; (×) a bump that has no effect; (△) a bump that has a weak effect on the convection patterns. The dashed line separates steady-state and time-dependent regimes. The classification is relevant only to the basal heating case. At the partly internal heating cases, the convection pattern becomes time-dependent when $Ra > 10^4$.

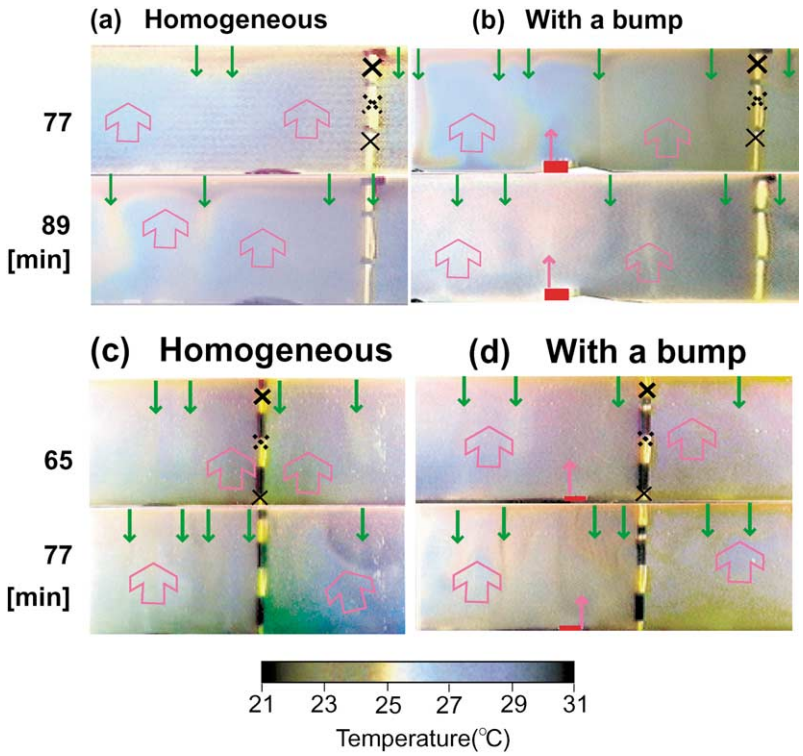

Fig. 3. Each panel is a snapshot of the temperature field visualized by thermotropic liquid crystal powder. Red/yellow parts correspond to low-temperature region (downwelling sites in a convection cell as shown by allows), while blue parts correspond to high-temperature region (upwellings). Temperatures lower than the red region and higher than the blue region are black because of the absence of reflection. The reflective color changes as a function of time because the core temperature of convection cells goes down. The numbers at the left-hand side indicate the time after the start of the boundary temperature lowers. Red marks show the location of the inserted bump, 10 mm width. The line of white beads is the thermistor array; (×) indicates the locations of thermistor probes.

Fig. 3 shows the temperature fields of the convection visualized by thermotropic liquid crystal powders. Fig. 3(a) shows the convection pattern with homogeneous boundary convection at $Ra_T \sim 3 \times 10^4$, $R \sim 6$, where the convection pattern is steady when $R \sim 0$. The heat flux by the convection of (a) is the same as that at $Ra_T \sim 10^6$ and $R \sim 0$. The convection pattern at $Ra_T \sim 10^6$, $R \sim 0$ also has no time dependency. Fig. 3(a), however, shows strongly time-dependent patterns. There are no vigorous ascending regions and no steady convecting cells. The locations of descending plumes are changeable, and the downwelling plumes have horizontal velocity. The convection pattern is also characterized by the width of each plume. The width of the plumes in (a) is the same order as that at the same Ra_T, $R \sim 0$, but is greater than that at $Ra_T \sim 10^6$, $R \sim 0$. Such a planform is consistent with the previous studies (Weinstein and Olson, 1990; Sotin and Labrosse, 1999). In this situation, there is no system to determine the locations of upwellings. Fig. 3(b) shows the temperature field of the convection pattern with a bump at the same values of Ra_T and R of (a). This shows that upwelling at the site of the bump survives longer than 12 min, which is the time scale of the plume emanation. These results indicate that the bump affects the convection pattern.

Fig. 3(c) and (d) shows the snapshots of the temperature field of convection patterns at higher $Ra_T \sim 5 \times 10^6$ and $R \sim 7$, which indicate narrower plumes and a more time-dependent feature than (a) and (b). Fig. 3(c) shows that cold plumes descend almost everywhere and that hot plumes are located where there

are no downwellings. The width of cold plumes is smaller than that of hot plumes, which indicates the broad feature of hot plumes. Cold plumes have distinct roots and stems; however, the roots of hot plumes are blurred. Hot and cold plumes never stay at the same locations; i.e. when a plume emanated from the boundary, the location of the root of the plume changes before the plume head reaches the other boundary. The width of each plume is the same as that at the same Ra_T, $R \sim 0$, and the time dependency is the same order as that at $Ra_T \sim 2 \times 10^7$, $R \sim 0$, where the transferred heat is the same as that at (c). On the other hand, (d) shows that the upwelling is steady only at the site of the bump. Except for the site of the bump, the upwellings are passive and broad. These results show that a bump of the same order of the critical height determined by the purely basal heating case affects the convection pattern under the partially internal heating case. The effect of the bump is weaker than that under purely basal heating. Under purely basal heating, the bump makes a steady convection cell at the site and anchors not only the location of the hot plume but also that of the neighboring cold plumes. Under the partially internal heating, however, the bump does not fix the location of neighboring cold plumes. Some cold plumes descend above the site of the bump, but a new upwelling is formed soon afterwards.

Next, we show how the plume activity (velocity, size, and emanation rate) is enhanced by the existence of the bump using the time-series measurements of the temperature. Fig. 4 is the time series of the temperature variation normalized by the imposed temperature difference and temperature lowering. Each spike-like temperature fluctuation indicates the horizontal and vertical passage of the plume. Spike-like temperature fluctuation includes three kinds of information about the passing plume, which are amplitude, number, and width. The amplitude of the spike shows the temperature difference between the inner and outer parts of the plume and indicates the magnitude of the buoyancy of the plume. The amplitudes of the temperature fluctuation of (b) and (d) are clearly larger than those of (a) and (c), respectively. Although in case (a), the visual observation of temperature field shows that some plumes pass beside the thermistor probes, the amplitude of temperature perturbation is much smaller than that of (b). This suggests that the existence of the bump produces temperature anomaly efficiently and

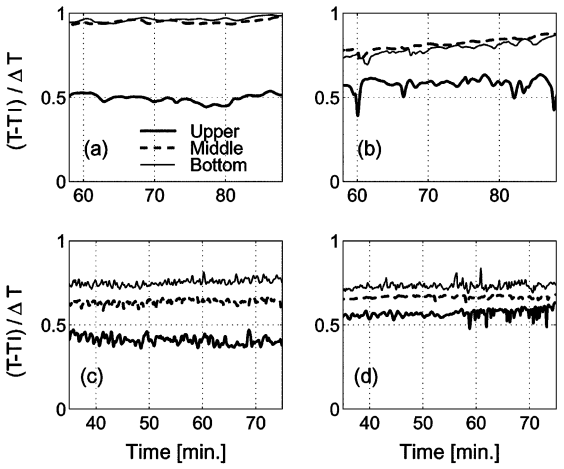

Fig. 4. Temperature variation as a function of time normalized by the imposed temperature difference and the imposed temperature lowering of boundaries. We fitted boundary temperature by a linear function. Thick, broken, and thin lines correspond to the location of probes at the upper, middle, and bottom of the convection cell (Fig. 3), respectively. Their normalized heights are 0.88, 0.57, and 0.29 in case (a) and (b), and 0.87, 0.50, and 0.05 in case (c) and (d). Time means the lapse after the start of boundary temperature lowering. The attached character corresponds to Fig. 3.

enhances the temperature contrast between the inner and outer parts of the plume. The enhanced temperature contrast is the source of the vigorous buoyancy.

The number of the spikes corresponds to the number of plumes. The number of spikes of (c) and (d) is higher than that of (a) and (b), respectively, which indicates that more plumes pass the probe as Ra_T increases under the same boundary conditions. Fig. 4 (b) and (d) show a higher number of spikes than that of (a) and (c), respectively, indicating that the number of plumes is increased by the existence of the bump.

The width of the spike-like temperature fluctuation gives information about the velocity of the plume and its size. If the plume velocity is high and the size is small, the width of the spike becomes narrow. The spikes of Fig. 4(a) and (b) are wider than those of (c) and (d), which means that the plume velocity becomes larger and its size becomes smaller as Ra_T increases. This is consistent with the visual observations. These features are clearly shown in Fig. 5, which is the temperature power spectra of the records shown in Fig. 4. High-frequency components correspond to the narrow width spikes. Comparisons between (a),

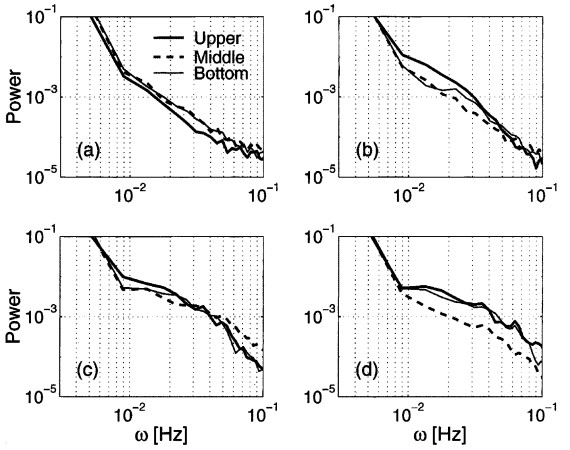

Fig. 5. The power spectra of the temperature shown in Fig. 4. Data length in calculation of the power corresponds to that shown in Fig. 4.

(b) and (c), (d), respectively, show that higher frequency components are enhanced as Ra_T increases under the same boundary conditions. We compared the power spectra of (b), (d) and (a), (c), respectively. The high-frequency components of temperature fluctuations near the upper and lower boundaries are enhanced by the existence of the bump. The width of each spike of Fig. 4(b) and (d) is also narrower than that of (a) and (c).

4. Discussion

4.1. The role of the internal heating to the critical height

The above-mentioned experimental results show that the bump affects the convection pattern when its height is the same order of the critical height determined by the basal heating case (Fig. 2). Here, we discuss how the internal heat source affects the critical height of the bump.

First, let us review how the fixation mechanism works in the basal heating case. The critical height of the bump under the basal heating is strongly scaled by the thickness of the thermal boundary layer. Since an almost isothermal bump higher than the boundary layer introduces a high-temperature anomaly above the boundary (approximately $\Delta T/2$) and the resulting lateral thermal anomaly is unstable, it becomes a site of upwelling. At the same time, the horizontal flow in the boundary layer is forced upward because of this bump, in which the thickness of the velocity boundary layer is the same order of that of the thermal boundary layer (Belmonte et al.,1994). Because of these coupled effects, the upwelling is strongly fixed at the position of the bump. The non-dimensional thickness of the thermal boundary layer in purely basal heating convection is estimated by

$$\delta = \frac{1}{2 \times Nu} = \frac{1}{2 \times \alpha Ra^{\beta}} \tag{4}$$

where α and β are the experimentally determined constants. This is the mean thickness of the thermal boundary layer. When the convection pattern is time-dependent, the critical height becomes smaller than the thickness estimated by Eq. (4). The thickness of the thermal boundary layer changes with time at a given location under the time-dependent convection. To fix the location of the upwelling, the bump should be thicker than the minimum thickness of the thermal boundary layer. The critical height is thus smaller than the mean thickness of the thermal boundary layer in the regime of time-dependent convection.

When the internal heating participates, the critical height should be also scaled by the thickness of the thermal boundary layer. In the following discussion, we estimate the thickness of the lower thermal boundary layer for the partially internal heating case. The thickness of the lower thermal boundary layer is a function of the heat flux that comes in the convection layer (Q_b) and the temperature difference across the boundary layer. In the basal heating case, the average temperature of the convection fluid is equal to the mean value of the imposed temperature difference for the sake of symmetry. Addition of internal heating breaks this symmetry and causes an increase of the average temperature. Sotin and Labrosse (1999) showed that the non-dimensional mean temperature of the convective fluid, T_m, is written as

$$T_m \sim 0.5 + 1.236 \frac{R^{3/4}}{Ra_T^{1/4}} \tag{5}$$

and the heat flux at the top boundary (Q_t) is

$$Q_t \sim 0.3446 Ra_T^{1/3} T_m^{4/3} \tag{6}$$

From the energy conservation, the heat flux at the bottom is denoted as

$$Q_{\mathrm{b}} \sim Q_{\mathrm{t}} - R \tag{7}$$

Since heat is transfered by conduction in the boundary layer, Q_{b} is also denoted by the Fourier's law

$$Q_{\mathrm{b}} \simeq \frac{1 - T_{\mathrm{m}}}{\delta_{\mathrm{b}}} \tag{8}$$

where δ_{b} is the non-dimensional thickness of the lower boundary layer. Inserting Eqs. (5)–(7) into Eq. (8) yields

$$\delta_{\mathrm{b}} \sim \frac{0.5 - 1.236R^{3/4}/Ra^{1/4}}{0.3446Ra^{1/3}(0.5 + 1.236R^{3/4}/Ra^{1/4})^{4/3} - R} \tag{9}$$

δ_{b} slightly decreases when R increases in the regime of $10^6 < Ra < 10^8$ and $R < 40$. This suggests that the critical height decreases as R increases in this region, yielding high sensitivity of convection pattern to the heterogeneity in the boundary region. This is consistent with our observation.

Moreover, the addition of internal heating makes convection patterns time-dependent at the same Ra_T. As mentioned before, time-dependent convection causes variation in the thickness of the thermal boundary layer. To affect the convection pattern, the bump has to exceed the minimum thickness of the thermal boundary layer. This effect will also decrease the critical height at the region $10^3 < Ra_T < 10^6$ classified as steady-state convection when $R \sim 0$.

4.2. Effect of the bump on plume activity and heat transfer

As shown in Figs. 4 and 5, the bump enhances the plume activity. The mechanism is considered as follows. Visual observations showed that the size of the upwelling at the site of the bump is larger than that at other upwellings, but they do not show remarkable difference of plume size between the plume at other site of the bump and that under the homogeneous boundary cases. The probe is not located right above the bump. The detected high-frequency components do not originate in the plume above the bump.

However, the effect of the obviously large plume at the site of the bump should spread to the surroundings. The coalescence of the hot fluid parcel into a large plume at the site of the bump exceeds the production of the hot fluid parcel by the growth of the thermal boundary layer. In order for a large plume to emanate continuously, the hot fluid parcels should be supplied not only by the site of the bump but also by the vicinity of the bump. The horizontal flow should be developed at the vicinity of the boundary to collect heated (cooled) fluid efficiently. Consequently, the high-frequency component is observed in the vicinity of the upper and lower boundaries and is not so obvious at the middle depth of the convection layer (Fig. 5).

Since the plume is a dominant carrier of heat, the bump might enhance the efficiency of the heat flux. There is some evidence to support this hypothesis. Although (a) and (b) are at the same Ra_T and R, the mean temperature of the convection layer of (a) is higher than that of (b) (see thin and dashed line of Fig. 4). The mean temperature of the convection cell is related with the ability of the heat transport. If the excess heat associated with the lowering of boundary temperature is efficiently transferred to the outside of the convection layer, the increase of the mean temperature is small. The lower mean temperature of (b) compared with (a) suggests the enhancement of the heat transport by the bump. In Fig. 4, the thick line in (d) shows temperature fluctuations characterized by downward spikes; however, that of (c) shows upward spikes. The absolute temperature of the thick line of (d) is higher than that of (c), despite these probes having the same height. It is inferred that, in case (d), the uppermost probe is located outside of the upper thermal boundary layer and that of (c) is located inside of the thermal boundary layer; i.e. the thickness of the thermal boundary layer is decreased by the bump.

The horizontal flow developed in the vicinity of the boundary should also enhance the heat transfer. In the vicinity of the lower boundary, there are many small hot plumes that emanate from the growth of the thermal boundary. The plumes do not have enough buoyancy to reach the other boundary because of their smallness. The small plumes are carried by the horizontal flow to the site of the bump, coalesce efficiently, and make a larger plume that has enough buoyancy to reach the upper boundary. The larger plumes transfer heat efficiently. The growth rate of the thermal boundary layer is enhanced at the same time, because the

heated fluid is always taken away by the horizontal flow, which also contributes to the promotion of the heat transfer.

These phenomena suggest that the bump brings about temperature anomaly, causes plumes to emanate efficiently, builds a mean flow at the vicinity of the boundary layer, and enhances the heat transfer. Du and Tong (2000) showed that heat transfer is enhanced by ordered rough boundaries. Although the boundary undulation used in this work is just a single bump, it is probable that the bump enhanced the heat transfer.

4.3. Implications for the mantle

We showed that internal heating does not make the critical height of the bump larger. Therefore, the fixation mechanism will work in the Earth's mantle, as we showed in our previous work. In Fig. 2, the y-axis at the right is scaled to the thickness of the mantle. Since the estimated Ra_T of the mantle is 10^6–10^8, undulation greater than 100 km can affect mantle convection. Since the observed thickness variety of the D″ layer reaches 340 km at maximum (Kendall and Shearer, 1994; Wysession et al., 1998), undulations at the top of the D″ layer should be sufficient to control the pattern of mantle convection.

The problem is whether the heterogeneity in the D″ layer matches the bump in our experiments. We consider two models that have been proposed to explain the origin of the D″ layer. One model proposes that the D″ layer is a dense layer enriched in Fe because of ongoing differentiation in the outer core and/or reactions between the iron alloy in the outer core and silicates in the mantle. In this situation, the thermal conductivity of the D″ layer will be enhanced because of the high content of Fe. Manga and Jeanloz (1996) showed that mantle convection can create thickness variations in the D″ layer in this situation. The D″ layer with high thermal conductivity and with horizontal thickness variation is the same as that in our experimental settings. In this model, the upwelling makes the topography which maintain the location of upwelling.

The other model considers the accumulated material from subducted slabs as the source of the D″ layer. As the cold lithosphere is carried down, it will depress the D″ boundary and displace material within the D″ layer. The warmer, displaced material will form a topographical high relative to the adjacent cold, subducted material, resulting in boundary topography that is isostatically maintained by the thermal density contrast. In this way, lateral temperature variations and topography are generated simultaneously. Our experimental results show that both effects, the horizontal temperature difference and the topographical high, can contribute to the generation of a hot plume. Thus, thickness variations in the D″ layer generated by an ancient subducted slab material should generate upwellings above "pile-up" structures. The coupling between the upwelling and the undulation of the boundary stabilizes the convection and will maintain the long-lived coherent structure (Montague et al., 1998; Montague and Kellogg, 2000).

The estimated fraction of internal heating has a wide spread of 40–90% (Schubert et al., 1980; Davies, 1988; Sleep, 1990; Honda, 1995). The experimental range of the internal heating (40 and 70%) is slightly smaller than that estimated for the Earth's mantle. If there is a thermal boundary layer above the D″ layer, this mechanism should operate. There is considerable evidence suggesting the existence of the thermal boundary layer above the top of the D″ layer, as follows: (i) several seismological observations show a decrease in seismic velocity above the D″ layer, which can be interpreted as the thermal boundary layer (e.g. Young and Lay, 1990; Garnero et al., 1993); (ii) the estimated temperature difference between the Earth's mantle and the outer core is extremely large and cannot be explained without the thermal boundary layer above the D″ layer (e.g. Boehler, 1996; Farnetani, 1997); (iii) temperature profiles developed by numerical experiments in appropriate parameters to the mantle show the existence of the lower thermal boundary (e.g. Tackley et al., 1994; Butler and Peltier, 2000); (iv) the mean temperature of the convection layer does not exceed the lower boundary temperature until $R < 20$ (Sotin and Labrosse, 1999), which means that the thermal boundary layer is developed at the lower boundary under the appropriate parameter range for the mantle.

The effect of spherical geometry of the Earth's mantle makes the critical height of the bump smaller. The difference of the areas between the upper and lower boundaries changes the ratio of the lower to the upper thermal boundary layer thickness. To simplify the problem, we show the case of $R \sim 0$. The energy balance between upper and lower boundaries is written

as

$$4\pi r_b^2 Q_b \sim 4\pi r_t^2 Q_t \tag{10}$$

where r_b and r_t are the radii of the bottom and top boundaries, respectively. Inserting Eq. (6) into Eq. (10) yields

$$r_b^{3/2} \Delta T_b \sim r_t^{3/2} \Delta T_t \tag{11}$$

From the Fourier's law

$$4\pi r_b^2 \left(k \frac{\Delta T_b}{\delta_b} \right) \sim 4\pi r_t^2 \left(k \frac{\Delta T_t}{\delta_t} \right) \tag{12}$$

Dividing Eq. (11) by Eq. (12) yields

$$\frac{\delta_b}{\delta_t} \sim \left(\frac{r_b}{r_t} \right)^{1/2} \tag{13}$$

Eq. (13) means that the ratio of the thickness of the lower and upper thermal boundaries depends on the ratio of their radii. In the case of the Earth's mantle, the thickness ratio made by radius ratio is 0.7, which slightly decreases the thickness of the lower thermal boundary.

In the basal heating case, the bump fixes the location of upwelling and elongates the convection cells, and no downwellings are observed at the site of the bump. On the other hand, in the internal heating case, some cold plumes descend above the site of the bump, but a new upwelling forms soon afterwards. The Earth's hotspot does not seem to control the global pattern of the mantle convection, and a subducting slab sometimes descends above the hotspot. This situation is similar to our experiments with internal heat sources.

The Earth's mantle is characterized by two different scales in upwellings. One is the degree two pattern shown by the seismic topography (Su et al., 1994), and the other consists of hotspots with a short length-scale. Numerous simulations suggest that the size of the upwelling is scaled by the thickness of the thermal boundary layer, but never show coexistence of different scales in upwellings in one convection layer. Our experiments show three kinds of upwellings, i.e. small plumes which cannot reach the other boundary by themselves, large plumes made of the coalescence of the small plumes, and plumes formed in response to the downwelling that has long wavelength. If these three types of upwellings exist in the Earth's mantle, only the last one will be detected by seismic tomography, since the former two upwellings are too small to be detected. The second one, the large plume, is recognized by volcanic activity. The first one, the small plumes, is never recognized from the surface of the Earth. This situation is depicted in Fig. 6. This seemingly independent coexistence of localized hotspots and global mantle convection flow can be explained by considering that hotspots are anchored by heterogeneities at the base of the mantle.

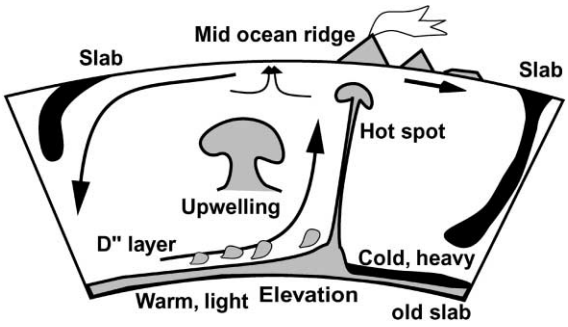

Fig. 6. Cartoon of three types of upwellings.

Acknowledgements

A.N. thanks Prof. P. Olson for discussions and his kind hospitality at Johns Hopkins University (USA), where part of this paper was written. We thank two anonymous reviewers for helpful advice. A.N. is supported by JSPS Research Fellowships for Young Scientists.

References

Belmonte, A., Tilgner, A., Libchaber, A., 1994. Temperature and velocity boundary layers in turbulent convection. Phys. Rev. E 50, 269–279.

Bercovici, D., Schubert, G., Glatzmaier, G.A., 1989. Influence of heating mode on three-dimensional mantle convection. Geophys. Res. Lett. 16, 617–620.

Boehler, R., 1996. Melting temperature of the Earth's mantle and core: Earth's thermal structure. Annu. Rev. Earth Planet. Sci. 24, 15–40.

Butler, S.L., Peltier, W.R., 2000. On scaling relations in time-dependent mantle convection and the heat transfer constraint on layering. J. Geophys. Res. 105, 3175–3208.

Davies, G.F., 1988. Role of the lithosphere in mantle convection. J. Geophys. Res. 93, 10451–10466.

Du, Y.B., Tong, P., 2000. Turbulent thermal convection in a cell with ordered rough boundaries. J. Fluid Mech. 407, 57–84.

Farnetani, C.G., 1997. Excess temperature of mantle plumes: the role of chemical statification across D″. Geophys. Res. Lett. 24, 1583–1586.

Garnero, E.J., 2000. Heterogeneity of the lowermost mantle. Annu. Rev. Earth Planet. Sci. 28, 509–537.

Garnero, E.J., Helmberger, D.V., Grand, S., 1993. Preliminary evidence for a lower mantle shear-wave velocity discontinuity beneath the central Pacific. Phys. Earth Planet. Int. 79, 335–347.

Hansen, U., Yuen, D.A., 1988. Numerical simulations of thermal–chemical instabilities at the core–mantle boundary. Nature 334, 237–240.

Honda, S., 1995. A simple parameterized model of Earth's thermal history with the transition from layered to whole mantle convection. Earth Planet. Sci. Lett. 131, 357–369.

Houseman, G., 1988. The dependence of convection planform on mode of heating. Nature 332, 346–349.

Kellogg, L.H., 1997. Growing the Earth's D″ layer: effect of density variations at the core–mantle boundary. Geophys. Res. Lett. 24, 2749–2752.

Kendall, J.M., Shearer, P.M., 1994. Lateral variations in D″ thickness from long-period shear-wave data. J. Geophys. Res. 99, 11575–11590.

Krishnamurti, R., 1968a. Finite amplitude convection with changing mean temperature. 1. Theory. J. Fluid Mech. 33, 445–455.

Krishnamurti, R., 1968b. Finite amplitude convection with changing mean temperature. 2. An experimental test of the theory. J. Fluid Mech. 33, 457–463.

Lay, T., Garnero, E.J., Young, C.J., Gaherty, J.B., 1997. Scale lengths of shear velocity heterogeneity at the base of the mantle from S wave differential travel times. J. Geophs. Res. 102, 9887–9909.

Manga, M., Jeanloz, R., 1996. Implications of a metal-bearing chemical boundary layer in D″ for mantle dynamics. Geophys. Res. Lett. 23, 3091–3094.

Montague, N.L., Kellogg, L.H., 2000. Numerical models of a dense layer at the base of the mantle and implications for the geodynamics of D″. J. Geophys. Res. 105, 11101–11114.

Montague, N.L., Kellogg, L.H., Manga, M., 1998. High Rayleigh number thermo-chemical models of a dense boundary layer in D″. Geophys. Res. Lett. 25, 2345–2348.

Namiki, A., Kurita, K., 1999. The influence of boundary heterogeneity in experimental models of mantle convection. Geophys. Res. Lett. 26, 1929–1932.

Olson, P., Kincaid, C., 1991. Experiments on the interaction of thermal convection and compositional layering at the base of the mantle. J. Geophys. Res. 96, 4347–4354.

Parmentier, E.M., Sotin, C., Travis, B.J., 1994. Turbulent 3-D thermal convection in an infinite Prandtl number, volumetrically heated fluid: implications for mantle dynamics. Geophys. J. Int. 116, 241–251.

Schubert, G., Stevenson, D., Cassen, P., 1980. Whole planet cooling and the radiogenic heat source contents of the Earth and Moon. J. Geophys. Res. 85, 2531–2538.

Serghiou, G., Zerr, A., Boehler, R., 1998. (Mg, Fe)SiO_3-perovskite stability under lower mantle conditions. Science 280, 2093–2095.

Shen, Y., Tong, P., Xia, K.-Q., 1996. Turbulent convection over rough surfaces. Phys. Rev. Lett. 76, 908–911.

Sidorin, I., Gurnis, M., Helmberger, D.V., 1999. Dynamics of a phase change at the base of the mantle consistent with seismological observations. J. Geophys. Res. 104, 15005–15023.

Sleep, N.H., 1990. Hotspots and mantle plumes: some phenomenology. J. Geophys. Res. 95, 6715–6736.

Sotin, C., Labrosse, S., 1999. Three-dimensional thermal convection in an *iso*-viscous, infinite Prandtl number fluid heated from within and from below: applications to the transfer of heat through planetary mantles. Phys. Earth Planet. Int. 112, 171–190.

Su, W.J., Woodward, R.L., Dziewonski, A.M., 1994. Degree-12 model of shear velocity heterogeneity in the mantle. J. Geophys. Res. 99, 6945–6980.

Tackley, P., Stevenson, D.J., Glatzmaier, G.A., Schubert, G., 1994. Effects of multiple phase transitions in a three-dimensional spherical model of convection in Earth's mantle. J. Geophys. Res. 99, 15877–15901.

Tackley, P.J., 1998. Three-dimensional simulations of mantle convection with a thermo-chemical basal boundary layer: D″? In: Gurnis, M., Wysession, M.E., Knittle, E., Buffett, B.A. (Eds.), The Core–Mantle Boundary Region. AGU, Washington, DC, pp. 231–253.

Travis, B., Weinstein, S., Olson, P., 1990. Three-dimensional convection planforms with internal heat generation. Geophys. Res. Lett. 17, 243–246.

Weinstein, S.A., Olson, P., 1990. Planforms in thermal convection with internal heat sources at large Rayleigh and Prandtl numbers. Geophys. Res. Lett. 17, 239–242.

Wysession, M.E., 1996. Large-scale structure at the core–mantle boundary from diffracted waves. Nature 382, 244–248.

Wysession, M.E., Lay, T., Revenaugh, J., Williams, Q., Garnero, E.J., Jeanloz, R., Kellogg, L.H., 1998. The D″ discontinuity and its implications. In: Gurnis, M., Wysession, M.E., Knittle, E., Buffett, B.A. (Eds.), The Core–Mantle Boundary Region. AGU, Washington, DC, pp. 273–297.

Young, C.J., Lay, T., 1990. Multiple phase-analysis of the shear velocity structure in the D″ region beneath Alaska. J. Geophys. Res. 95, 17385–17402.